ISSN 1070-3632, Russian Journal of General Chemistry, 2013, Vol. 83, No. 11, pp. 2132–2147. © Pleiades Publishing, Ltd., 2013.
Original Russian Text © M.I. Samoilovich, A.B. Rinkevich, V. Bovtun, A.F. Belyanin, M. Kempa, D. Nuzhnyy, M.Yu. Tsvetkov, S.M. Kleshcheva, 2012, published in Rossiiskii Khimicheskii Zhurnal, 2012, Vol. 56, Nos. 1–2, pp. 11–25.

Optical, Magnetic, and Dielectric Properties of Opal Matrices with Intersphere Nanocavities Filled with Crystalline Multiferroic, Piezoelectric, and Segnetoelectric Materials

M. I. Samoilovich[a], A. B. Rinkevich[b], V. Bovtun[c], A. F. Belyanin[a], M. Kempa[c], D. Nuzhnyy[c], M. Yu. Tsvetkov[a], and S. M. Kleshcheva[a]

[a] *Tekhnomash Central Research Institute of Technology, ul. Ivana Franko 4, Moscow, 121108 Russia*
[b] *Institute of Metal Physics, Ural Branch, Russian Academy of Sciences, Yekaterinburg, Russia*
e-mail: rin@imp.uran.ru
[c] *Institute of Physics ASCR, Na Slovance 2, Praha 8, 18221 Czech Republic*

Received June 1, 2012

Abstract—The properties and structure of composites on the basis of the lattice packings of SiO_2 nanospheres (opal matrices), containing in intersphere nanocavities clusters of the crystal phases of multiferroics and piezoelectric and ferroelectric materials.

DOI: 10.1134/S1070363213110339

INTRODUCTION

One of the lines of realization of the application of multiferroics, specifically magnetically ordered toroidal structures or ferrotoroidally order (FTO) systems, is their preparation and research. Multiferroic materials and metamaterials (which have only recently come under the scrutiny of science) hold promise for the creation of devices based on magneto- and electro-optical effects. It is suggested that due to spontaneous magnetization in a local electric field, inherent in these materials, along with polarization in magnetic fields, multiferroic materials of this type will find wide application in microelectronics and various sensor devices, as well as such a new progressing field as spin electronics (spintronics). Of particular interest are the works dealing with preparation and research of multiferroid materials as ordered 3D nanolattices of 15–40-nm crystallites with crystalline rare-earth metal manganite, phosphate, cuprite, and titanate nanoparticles embedded in their intersphere nanocavities.

It can be suggested that just the development and use of such multiferroid metamaterials will make it possible to create systems functioning at room temperatures. In this connection basic research on new types of multiferroics and multiferroid materials with preset properties (propagation of electromagnetic waves, as well as dielectric, electro-optical, magneto-optical, magnetic, and other characteristics) is required. In particular, experiments on the synthesis of high-quality lattice packings of 180−380-nm SiO_2 nanospheres (opal matrices) are necessary. The goal of such experiments is to understand and control the interrelationship between the electric and magnetic parameters of practically promising multiferroics of this type.

However, even though a great number of works on the synthesis and study of ferrotoroidal multiferroics of different compositions have been reported, the most part of the synthesized and studied materials are hardly suitable for practical application. These materials not always possess spontaneous magnetization (or polarization), and, moreover, they exhibit the required properties only at low temperatures or the values of the parameters of interest are lower (by two or more orders of magnitude) than required.

The above-mentioned objects for study, specifically opal matrices, are lattice packings (generally, cubic) of X-ray amorphous SoO_2 nanospheres with close diameters ($\Delta d < 5\%$); the size of the SiO_2 nanospheres varies from 200 to 400 nm, depending on their formation conditions. In the present work we studied the composition, optical, magnetic, and dielectric properties of nanocomposites on the basis of opal matrices with crystalline multiferroics, crystallites of rare-earth metal titanates like $R_2Ti_2O_7$ or R_2TiO_5, and

crystal phases of piezo- and segnetoelectric materials (ZnO, $BaTiO_3$, and $PbTiO_3$), embedded in their intersperical voids. There are strong reasons to suggest that such materials will be useful in devices for controlling phase velocities and electromagnetic radiation profiles in the optical, SHF, and THz ranges [1, 2].

Synthesis and Chemical Composition and Structure of Opal Matrices with Filled Intersphere Voids

The synthesis of opal matrices with SiO_2 nanosphere dimaters of 200−350 nm have been described in a number of publications (see, for example, [3−7]). The first stage involves solvolysis of tetraethyl orthosilicate $Si(OC_2H_5)_4$ with an ethanol solution in the presence of a catalyst (ammonium hydrate) to obtain X-ray amorphous SiO_2 nanoparticles which undergo polycondensation and acquire a spherical shape. The suspension was allowed to settle to form a hydrogel with a liquid content of up to 50−60 wt %, which transforms into a chalky and brittle material after drying. The resulting opal matrix is subjected to thermal treatment for removing residual water and hardening.

The densest packing of SiO_2 nanospheres has intersphere tetrahedral and octahedral voids (from 50 to 150 nm for the above-mentioned size of nanospheres) which can be filled with different substances. Technologies of the production of opal-based composites and magnetically, optically, and electrically (segneto-, piezo-) active materials with the spatial electric and dielectric dispersions varying in the range 150−300 nm have been developed.

One of the simplest methods of embedding chemical components into intersphere nanocavities of opal matrices is based on impregnation of a precursor substance solution of a definite chemical composition followed by thermal treatment during which particles of a required composition are formed in the matrix nanocavities. Precursor substances should be well soluble in water (or in other solvents) and transform into oxides at moderate temperatures of thermal treatment so that not to destroy the nanosphere packing. In our work we used as precursors water-soluble nitrates and other metal salts, as well as titanium trichloride in a weak HCl. During impregnation salt solutions fill voids in the opal matrix due to the capillary effect. The subsequent thermal treatment is performed at 600−900°C. This procedure is repeated many times (up to 20), which ensure gradual filling of intersphere nanocavities of the opal matrix.

The filling degree of intersphere nanocavities depends on the number of impregnations (increases from 15−20% after one impregnation to 40−50% after 10−20 impregnations). Thermal treatment leads to partial thermal degradation of compounds to be embedded and complete removal of unstructured water. Further on high-temperature thermal treatment is performed at 700−1200°C, depending on the stability range of the desired crystal phase for the chosen material.

The problem of the synthesis of metamaterials on the basis disperse media is quite difficult to solve because of the lack of data on the behavior of X-ray amorphous and crystal phases of substances in nanocavities of opal matrices at various temperatures and precursor concentrations. In particular, it was shown previously that the phase relations in such substances substantially (the corresponding phase fields are shifted by up to 400−500°C to a lower temperature) differ from what is observed in the phase diagram for bulk samples of the same composition and structure. Consequently, one has not only to develop procedures for embedding substances in nanocavities in a matrix, but also to establish stable crystallization ranges (by thermal treatment conditions), temperature ranges for the initiation of a reaction of substances accelerating crystallization in silicate systems, such as Pb and Zn, with X-ray amorphous silica to form silicates. The temperature ranges where X-ray amorphous silica starts to form crystal phases (primarily cristobalite) should be established. The high tolerance of opal matrices to thermal treatment allows studies to be performed at 500−1200°C.

Opal Matrices with Embedded Crystalline Multiferroics

We obtained mechanically and thermally strong opal matrices, which allowed us to fulfill required studies of above-mentioned types of dielectric metamaterials as potential multiferroid media on the basis of lattice packing of SiO_2 nanospheres with intersphere nanovoilds filled with toroidal multiferroics, such as $LiCoPO_4$, $LiNiPO_4$, $LiCuO_2$, etc. The main structural feature of FTO systems is toroidal ion spin ordering (Fig. 1).

Classical crystallography is, in principle, unable to represent the symmetry of such objects, since it is defined by an assembly of simplicial (cellular) complexes from topological structural units. Therefore, Nefedov's symmetries [8] are the only that allow

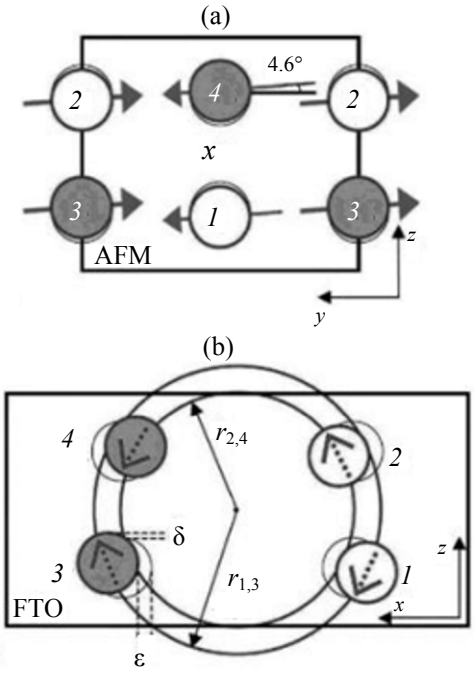

Fig. 1. Ordering of Co^{2+} ion spins on the (a) *yz* and (b) *xz* planes for the ground state of a crystalline multiferroic $LiCoPO_4$ [9]. AFM (FTO) stand for the antiferromagnetic (ferrotoroidal) order. Solid (open) circles are Co^{2+} ions for $x \sim 3/4$ (~1/4). The arrows show the spin components of Co^{2+} ions.

representation of the regularities of ordering in the electronic subsystem of multiferroics.

The composites on the basis of lattice packings of X-ray amorphous silica nanospheres were synthesized by a liquid phase technique, namely, by impregnating opal matrices with solutions of $LiNiPO_4$, $LiCoPO_4$, and $LiCuO_2$ multiferroics or an aqueous solution of $LiNO_3 \cdot 3H_2O$, followed by annealing at temperatures from 400°C to 1000°C.

The phase composition of the resulting composites was determined by X-ray diffraction on DRON-3M and XRD-6000 diffractometers (CuK_α radiation, graphite monochromator; no sample rotation, step 0.02°; continuous sample spinning, 1deg/min); an ICDD PDF-2 automated database was used. The results of the X-ray diffraction analysis of the opal matrices allows us to draw the following conclusions. The $LiCuO_2$ crystal phase (monoclinic syngony, space group *C*2/*m)* is formed at the annealing temperatures 750–1000°C (Fig. 2). Depending on the annealing temperature, along with $LiCuO_2$, the following phases are formed: SiO_2−quartz (hexagonal syngony, $P3_221$); CuO (monoclinic syngony, *Cc*), and Li_2O (cubic syngony, *Fm*-3*m*) (Fig. 2a).

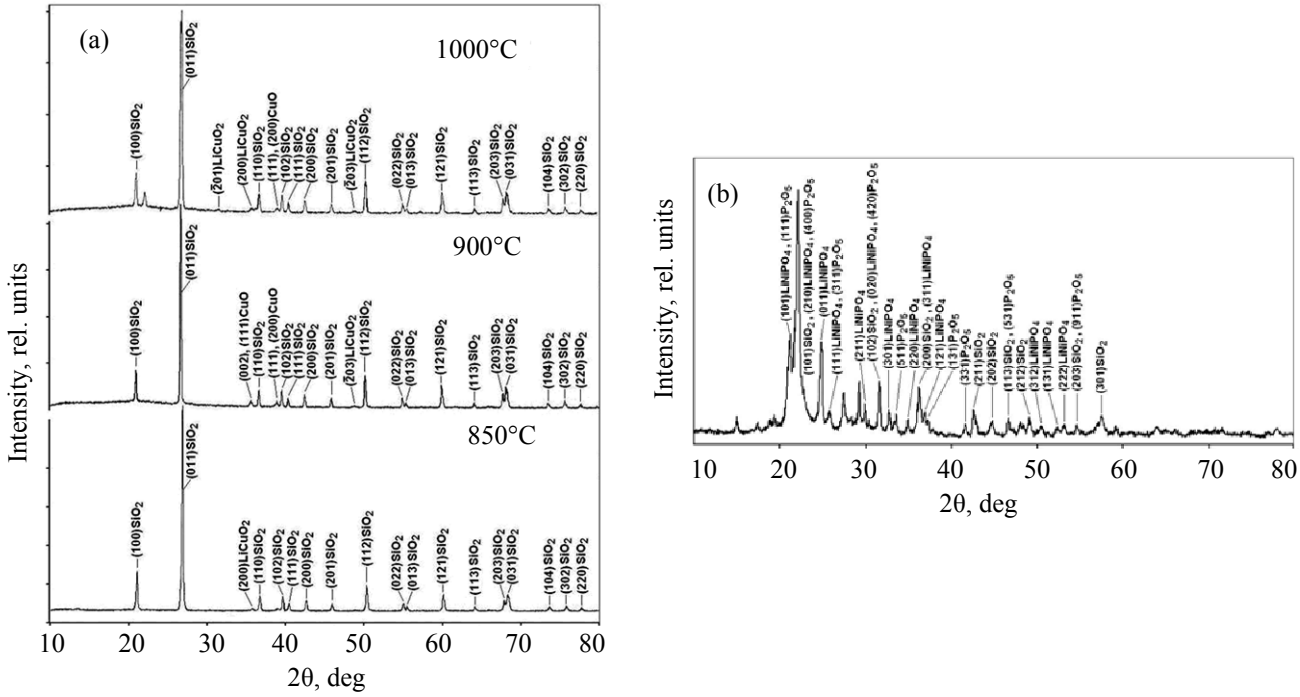

Fig. 2. X-ray diffraction patterns of the opal matrices with (a) Li and Cu ($LiCuO_2$, etc.) and (b) Li, Ni, and P compounds ($LiNiPO_4$, etc.) synthesized in their nanocavities. (a) The inserts show the synthesis temperature.

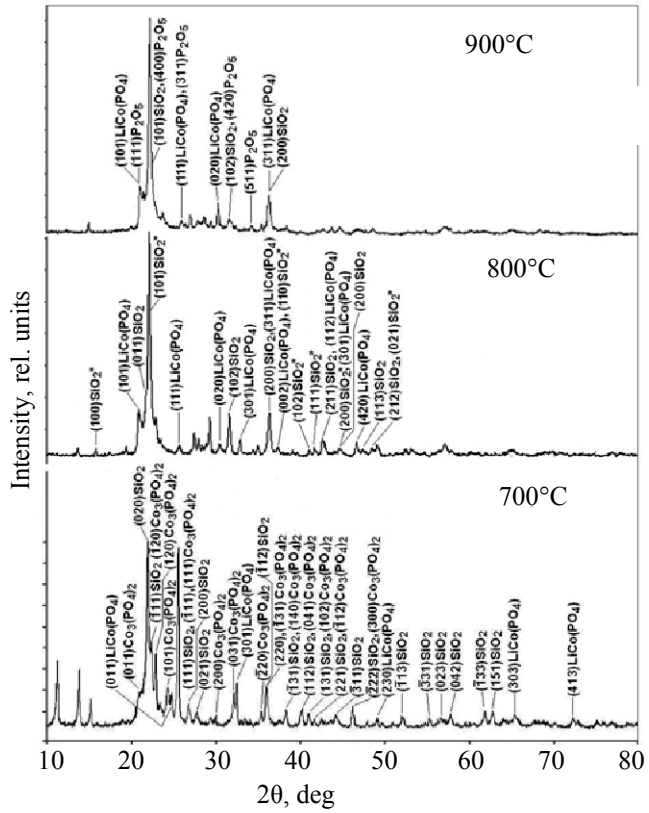

Fig. 3. X-ray diffraction patterns of the opal matrices with Li, Co, and P compounds ($LiCoPO_4$, etc.) synthesized in their nanocavities.

The $LiCuO_2$ crystal phase begins to form at temperatures above 750°C, and its concentration increases with temperature, and, therewith, recrystallization of SiO_2 is activated, and the concentration of the CuO phase decreases. About 800°C, a Li_2O phase is formed. Analogous results were obtained for phase formation in the opal matrices containing in their intersphere nanocavities on the basis of Li and Ni (phosphates). The phosphate $LiNi_2(P_3O_{10})$ was synthesized (monoclinic syngony, $P2_1/m$) (AFM structure), whereas $LiNiPO_4$ in low concentrations was observed (Fig. 2b) only when a mixture of orthophosphoric acid and aqueous ammonia was used as the solvent.

The $LiCoPO_4$ phase (orthorhombic syngony, *Pnma*) is formed in opal matrices at the annealing temperatures 700–900°C. Depending on the annealing temperature, along with $LiCoPO_4$, the following phases are formed: SiO_2 (monoclinic syngony), SiO_2 (cristobalite, tetragonal syngony, $P4_12_12$); $Co_3(PO_4)_2$ (monoclinic syngony, $P2_1/b$) (Fig. 3). The $LiCoPO_4$ crystal phase begins to form at temperatures above 500°C, and its highest concentration is observed in the samples of opal matrices annealed above 800°C.

The compositions of impregnating solutions and the conditions of thermal treatment were found, which allow a single-phase system ($LiCoPO_4$ crystal phase) to

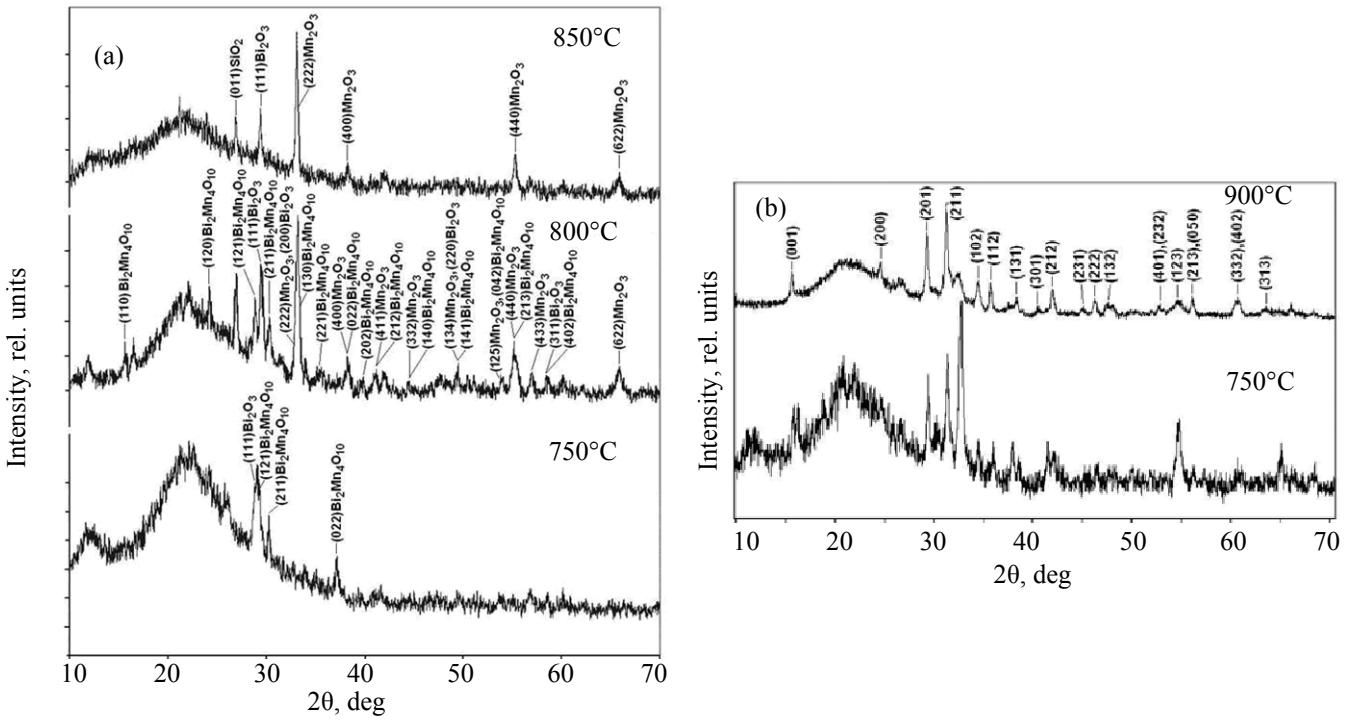

Fig. 4. X-ray diffraction patterns of the opal matrices with (a) Mn and Bi ($Bi_2Mn_4O_{10}$, etc.) and (b) $YMnO_3$ synthesized in their nanocavities.

be obtained in nanovoids. Simultaneously, works on embedding in opal matrices such compounds as $InFeO_3$ and $InMnO_3$ (isostructural to $GaFeO_3$) were performed. (The principal results of these works will be reported later, because we still failed to obtain single-phase systems, specifically those containing, for example, exclusively $InFeO_3$; various nanmagnetic and electrically inactive SiO_2 phases do not "interfere").

The substances synthesized in intersphere voids of opal matrices can be present in the X-ray amorphous or crystal states, and, therewith, the functional characteristics of the composites depend exclusively on the crystal phases.

Opal Matrices with Embedded Rare-Earth Metal Manganites

Nanocomposites on the basis of opal matrices with intersphere nanocavities filled with rare-earth metal manganites $RMnO_3$ or RMn_2O_5 (where R = Yb, Tb, Er, La, Y, Gd, Nd), as well as tungsten manganite were prepared by impregnation followed by thermal treatment. The X-ray diffraction patterns of the resulting samples are shown in Figs. 4 and 5.

The X-ray phase analysis showed that opal matrices with Mn−rare-earth metal compounds synthesized in their nanovoilds contain, along with the SiO_2 phase (hexagonal syngony, space group $P3_221$), the

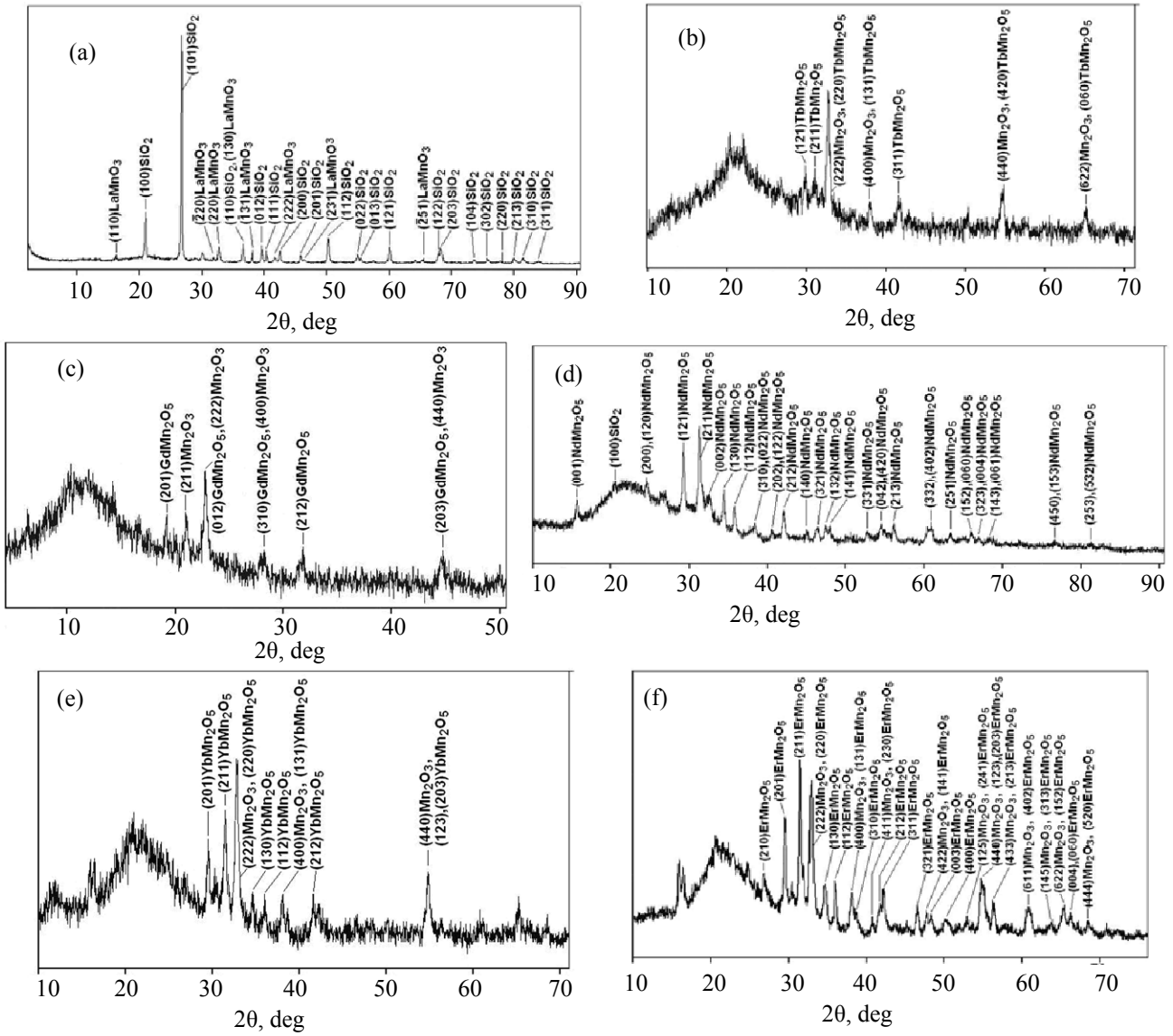

Fig. 5. X-ray diffraction patterns of the opal matrices with (a) $LaMnO_3$, (b) $TbMn_2O_5$, (c) $GdMn_2O_5$, (d) $NdMn_2O_5$, (e) $YbMn_2O_5$, and (f) $ErMn_2O_5$ clusters filling their intersphere nanocavities.

following crystal phases: Mn_2O_3 (cubic syngony, *Ia*-3), $ErMn_2O_5$ (orthorhombic syngony, *Pbam*), $YMnO_3$ (hexagonal syngony, *P*63*cm*), $LaMnO_3$ (rhombohedral syngony, *R*-3*c*), $GdMn_2O_5$ (orthorhombic syngony), $YbMn_2O_5$ (orthorhombic syngony, *Pbam*), $TbMn_2O_5$ (orthorhombic syngony, *Pbam*), and $NdMn_2O_5$ (orthorhombic syngony, *Pbam*). The sizes of crystallites (coherent X-ray scattering regions, CSR) in the directions perpendicular to the crystallographic planes {*hk*l} were determined by the broadening (half-width of the diffraction maximum) on the X-ray patterns of reflection from the {*hk*l} planes: $L_{circ} = k\lambda/\beta\cos\theta_{hkl}$, where *k* is a constant; λ, X-ray radiation wavelength; β, reflection broadening; and θ_{hkl}, reflection diffraction angle.

The synthesized materials have L_{circ} in the range 12–28 nm and a nearly equiaxial particle shapes.

Opal Matrices with Embedded Rare-Earth Metal Titanates

The results of X-ray diffraction analysis of the opal matrices with titanates like $R_2Ti_2O_7$ or R_2TiO_5 embedded in their intersphere nanovoids are shown in Fig. 6. The following crystal phases were found in the nanocavities: $Gd_2Ti_2O_7$ (cubic syngony, space group *Fd*3*m*), $Tb_2Ti_2O_7$ (cubic syngony, *Fd*3*m*), $Dy_2Ti_2O_7$ (cubic syngony, *Fd*3*m*), $Yb_2Ti_2O_7$ (cubic syngony, *Fd*3*m*), $Pr_2Ti_2O_7$ (monoclinic syngony, $P2_1$), and Er_2TiO_5 (hexagonal syngony); titanium oxides, specifically TiO_2 (rutile, tetragonal syngony, $P4_2/mnm$), $Ti_{0.72}O_2$ (synthetic anatase, tetragonal syngony, I41/*amd*), were also found in minor amounts. Moreover, as seen from the X-ray patterns, high-temperature treatment forms small amounts of the following crystal phases: SiO_2: SiO_2 (cristobalite, tetragonal syngony, $P4_12_12$) (Fig. 6a, curve *3* and Fig. 6b, curve *1*), SiO_2* (trimidite, hexagonal syngony, $P6_3/mmc$) (Fig. 6b, curve *1*), and SiO_2 (monoclinic syngony, *I*2/*a*) (Fig. 6b, curve *2*), which do not affect the magnetic or electric properties of the samples.

The nanoparticles formed in intersphere nano-voids comprise crystal and X-ray amorphous phases. The degree of crystallinity (fraction of the crystal phase in substance bulk) depends on the conditions of thermal treatment and varies from 0 (X-ray amorphous phases) to >90 vol %.

It was found that the size of crystallites (coherent scattering regions, CSR) in the crystal phases, which

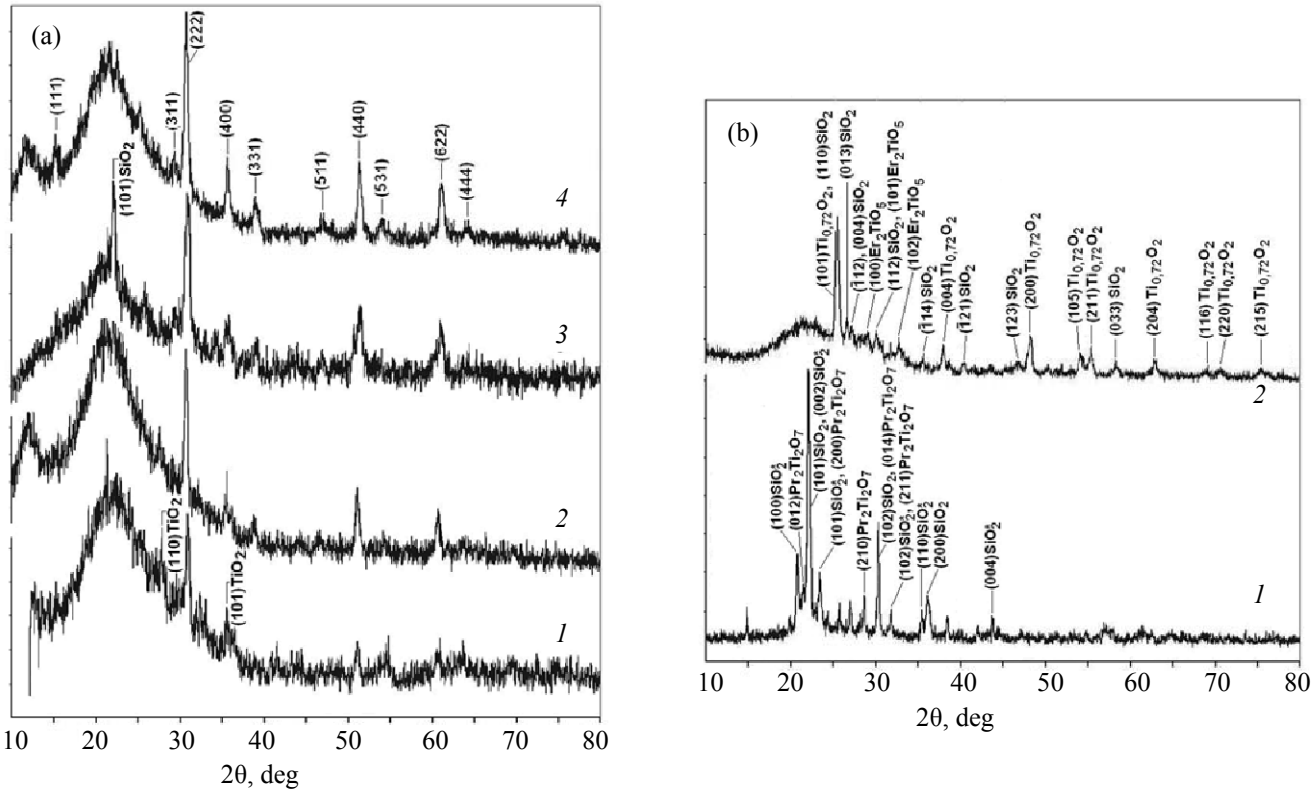

Fig. 6. X-ray diffraction patterns of the opal matrices with titanate clusters synthesized in their intersphere nanocavities. (a): (*1*) $Gd_2Ti_2O_7$, (*2*) $Tb_2Ti_2O_7$, (*3*) $Dy_2Ti_2O_7$, and (*4*) $Yb_2Ti_2O_7$ (all have cubic syngony crystals, space group *Fd*3*m*); (b): (*1*) $Pr_2Ti_2O_7$ (monoclinic syngony, *P*21) and (*2*) Er_2TiO_5 (hexagonal syngony).

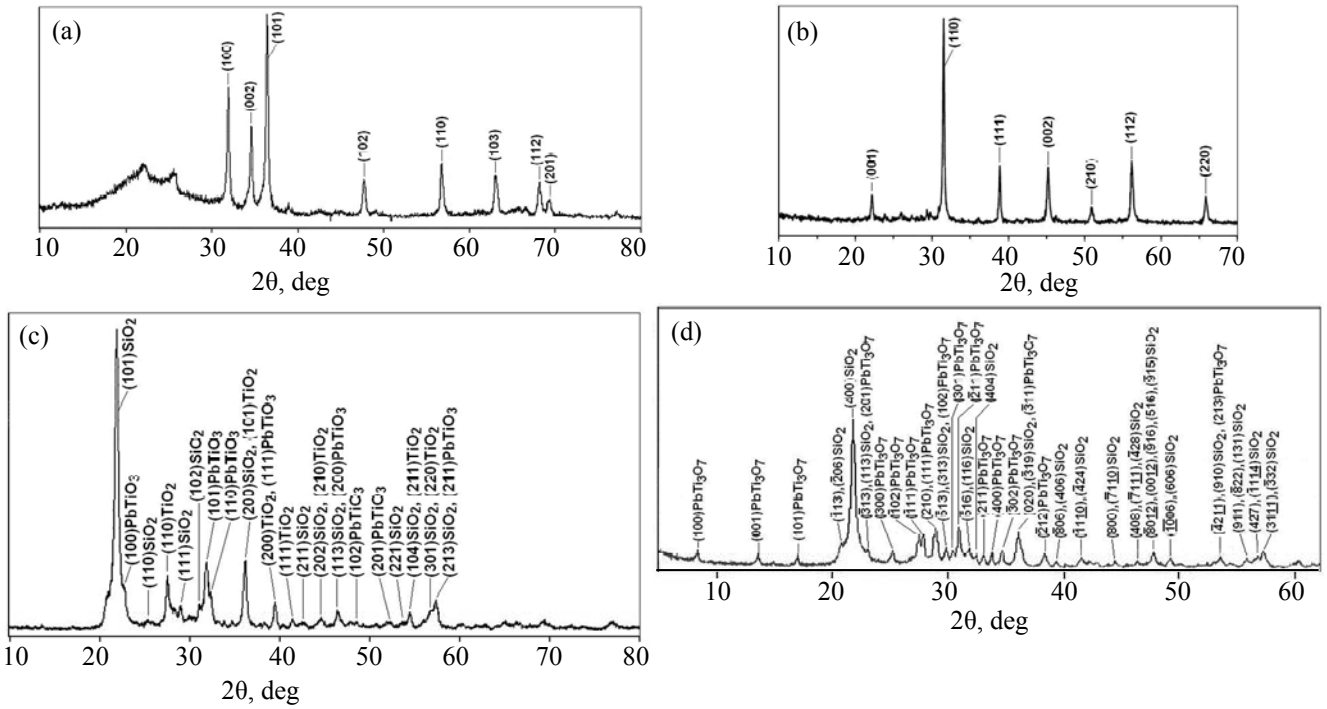

Fig. 7. X-ray diffraction patterns of opal matrices with (a) ZnO, (b) $BaTiO_3$, (c) $PbTiO_3$, and (d) $PbTi_3O_7$ clusters synthesized in their intersphere voids.

was determined from the broadening of X-ray diffraction maxima, is independent of the crystallinity degree of the synthesized substance. The CSR size in the substances synthesized in intersphere nanovoids spanned the range 12–37 nm; in particular, the CSR sizes for the substances with a cubic lattice (Fig. 6a) were as follows, nm: 22.7−36.2 ($Gd_2Ti_2O_7$), 19.6–22.8 ($Tb_2Ti_2O_7$), 15.6–21.5 ($Dy_2Ti_2O_7$), and 20.4–22.1 ($Yb_2Ti_2O_7$). Crystallites of the most part of the synthesized compounds have a close-to-equiaxial shape, and only $Gd_2Ti_2O_7$, $Tb_2Ti_2O_7$, and $Yb_2Ti_2O_7$ crystallites are slightly stretched along the <100> direction.

Opal Matrices with Embedded Piezoelectric Phases

Nanocomposites on the basis of opal matrices having interpherical nanocavities filled with ZnO, $BaTiO_3$, $PbTiO_3$, and $PbTi_3O_7$ crystal phases were synthesized by multiple impregnations followed by thermal treatment.

The phase composition of the samples was determined by X-ray diffraction analysis. The real structure was studied by high-resolution transmission electron microscopy (JEM-200C instrument). The X-ray phase analysis revealed the following crystal phases (Fig. 7): ZnO (hexagonal syngony, $P6_3mc$); $BaTiO_3$ (perovskite, tetragonal syngony, $P4mm$); $PbTiO_3$ (tetragonal syngony, $P4mm$), $PbTi_3O_7$ (monoclinic syngony, $P21$), as well as different titanium oxides, in particular, TiO_2 (rutile, tetragonal syngony, $P4_2/mnm$; $Ti_{0.72}O_2$ (synthetic anatase, tetragonal syngony, I41/*amd*).

Moreover, as seen from the X-ray diffraction patterns in Fig. 7, high-temperature annealing forms SiO_2 crystal phases which have no effect on the electric properties of the samples. Under certain conditions, a $Ba_6Ti_{17}O_{40}$ phase is formed (monoclinic syngony, $A2/a$). Sometimes the substance synthesized in nanocavities reacted with silica. In zinc oxide–embedded opal matrices annealed under certain conditions we detected a Zn_2SiO_4 phase (willemite, trigonal syngony, $R3$).

The nanoparticles formed in intersphere nanocavities comprise crystal and X-ray amorphous phases but their ratio could not be determined. The crystallinity degree depends on thermal treatment conditions and varies from 0 (X-ray amorphous phases) to >90 vol %. The coherent X-ray scattering regions of the crystal phases in intersphere voids depend on the crystallinity degrees of the synthesized materials and comprise 18–47 nm.

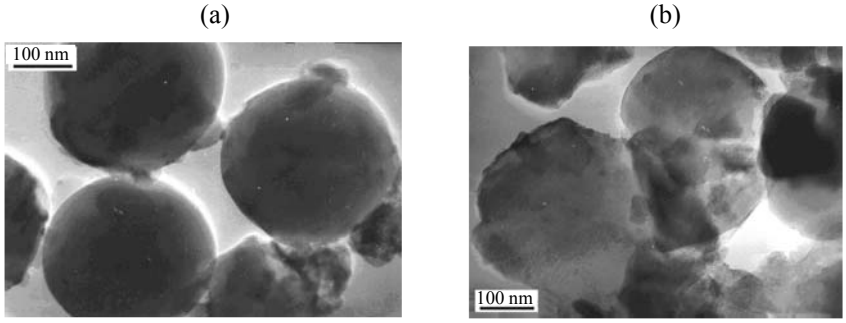

Fig. 8. Structure of opal matrices with (a) Ti oxide and (b) Zn oxide clusters synthesized in their intersphere nanocavities with simultaneous formation of $Zn_2Si_3O_5$.

With titanium-containing salts introduced into the matrix, polycrystalline TiO_2 particles are most commonly formed at temperatures above 800°C, and, therewith, the synthesized material does not react with SiO_2 nanospheres (Fig. 8). Transmission electron microscopy makes it possible to differentiate SiO_2 nanospheres and nanoparticles embedded in interspherical voids. If nanocavities are filled completely, inclusions not infrequently have the shape of tetrahedra or octahedra (Fig. 8a). The phase composition and structure of the synthesized materials depend on the composition of the impregnating solution, precursor concentration, and annealing conditions after impregnation. When silicate-forming substances are synthesized in nanocavities, they react with silica, and, therewith, SiO_2 nanospheres are deformed, which, as seen in Fig. 8, takes place with ZnO-containing samples but only slightly expressed in the case of Ba and Pb oxides.

Optical Characterisrics of Nanocomposites

We have studied the optical properties (Raman and reflection spectra) of a series of opal matrices with ferroic, manganite, titanate, phosphate, and cuprate clusters and segneto- and piezoelectric crystal phases embedded in their intersphere nanocavities. The optical spectra were measured on a LabRam HR800 micro Raman spectrometer (HORIBA Jobin-Yvon) and UV-3600 spectrophotometer (Shimadzu).

Figures 9–11 show the Raman spectra of certain samples. The spectra in Fig. 10 show bands characteristic of the crystal phase in intersphere nanocavities, specified in the legend to this figure, as well as manganese oxides, in some cases.

The reflection spectra in the optical range of opal matrices with crystal phases confined in interspherical nanocavities are shown in Figs. 12–14.

Magnetic properties of nanocomposites

Magnetic measurements were performed on a Quantum Design MPMS-XL device at field strengths of up to 50 kOe and temperatures from 2 to 300 K [9]. Magnetization curves and hysteresis loops, as well as temperature dependences of magnetic moments at a field strength of 10 kOe were measured. The results were analyzed taking into account the phase compositions and structural and magnetic states of nanocomposites.

A good reproducibility of magnetic measurements is worth noting.

The magnetization curve of the opal matrix filled with $LiCoPO_4$ nanoparticles, measured at room

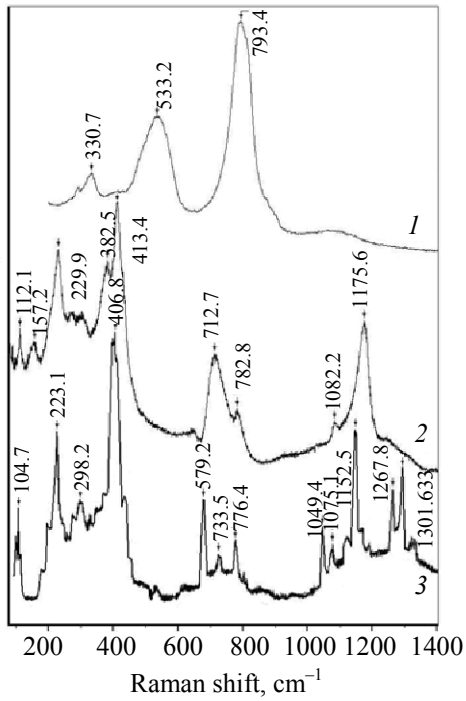

Fig. 9. Raman spectra of the opal matrices with (*1*) $LiCuO_2$, etc.; (*2*) $LiNiPO_4$; and (*3*) $LiCoPO_4$ clusters filling their intersphere nanocavities.

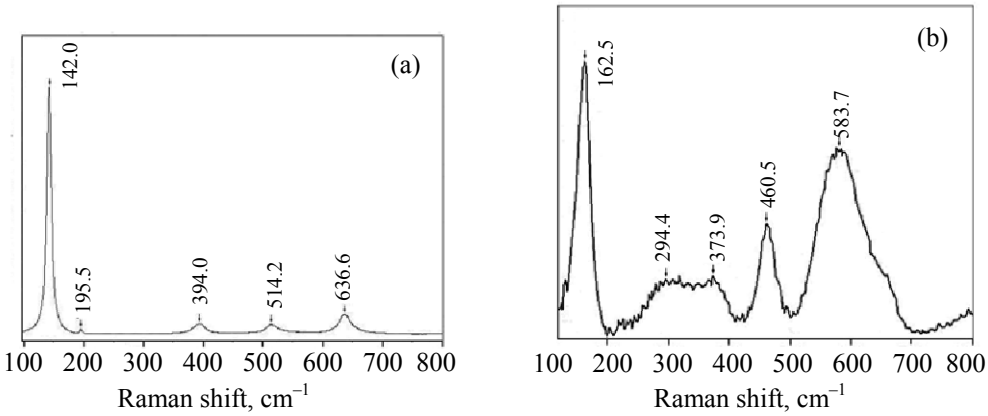

Fig. 10. Raman spectra of the opal matrices with (a) $LaMnO_3$ and (b) $Bi_2Mn_4O_{10}$ clusters filling their intersphere nanocavities.

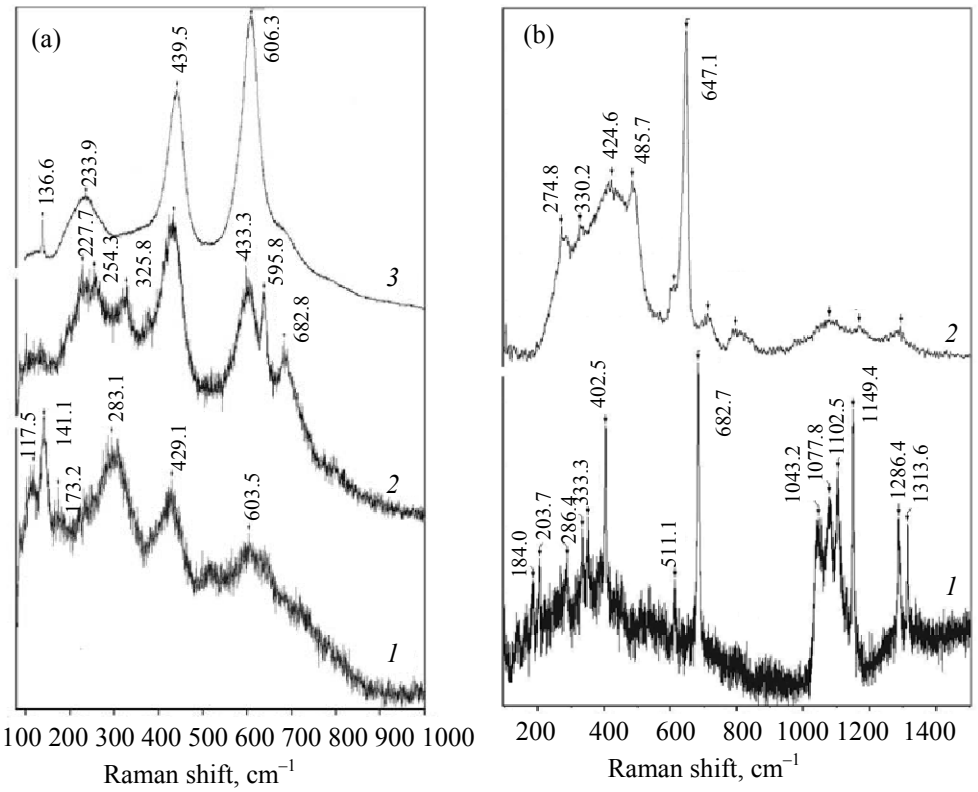

Fig. 11. Raman spectra of the opal matrices with (a): (*1*) $Dy_2Ti_2O_7$, (*2*) $Gd_2Ti_2O_7$, (*3*) $Yb_2Ti_2O_7$, (b) (*1*) $Pr_2Ti_2O_7$, and (*2*) $Tb_2Ti_2O_7$ clusters filling their intersphere nanocavities.

temperature (Fig. 15), showed no signs of saturation, and, therewith, the coercitive force is much lower than at T = 2 K. The general tendency of magnetic susceptibility to decrease with temperature is preserved, but the measurement uncertainties are too large to allow judgments on some peculiarities at T = 50 K. The imaginary magnetic susceptibility is much lower than the real magnetic susceptibility and is measured with a larger uncertainty.

Analysis of the magnetization curves suggests that the nanocomposites exhibit both ferrimagnetic and superparamagnetic. The superparamagnetism can be explained by the presence of small metal nanoparticles

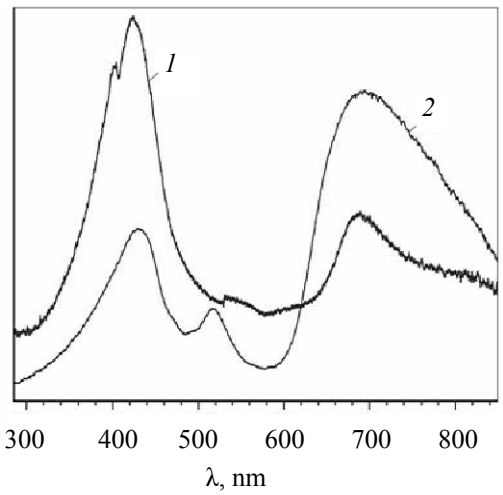

Fig. 12. Reflection spectra of the opal matrices with (*1*) $LiNiPO_4$ and (*2*) $LiCoPO_4$ clusters filling their interspherical nanocavities.

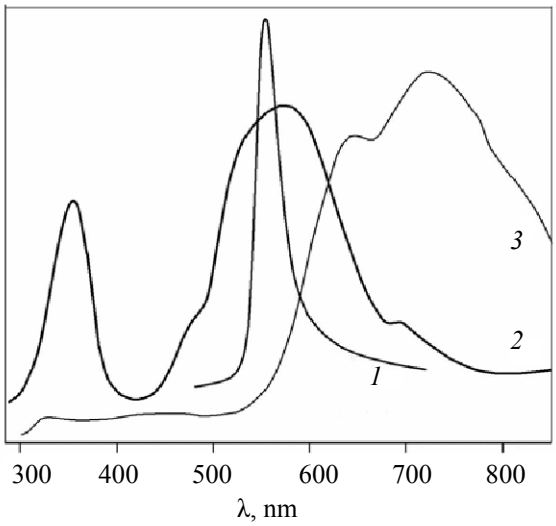

Fig. 13. Reflection spectra of (*1*) $La_2Ti_2O_7$, (*2*) $Pr_2Ti_2O_7$, and (*3*) Er_2TiO_5 clusters filling their intersphere nanocavities.

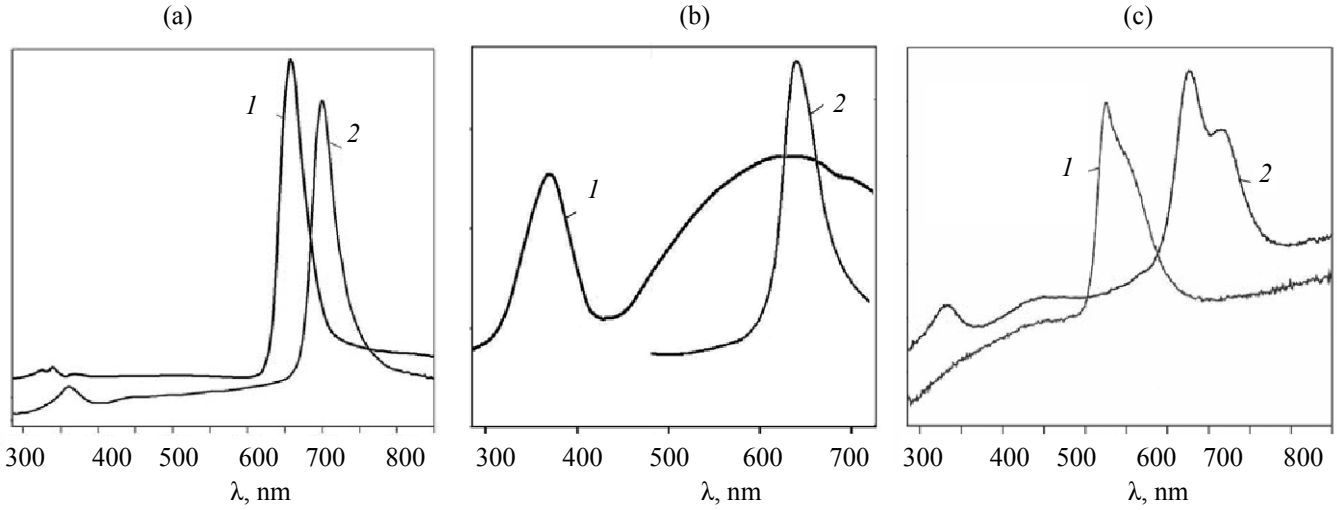

Fig. 14. Reflection spectra of (a) (*1*) $GdMn_2O_5$, (*2*) $ErMn_2O_5$, (b) (*1*) $Bi_2Mn_4O_{10}$, (*2*) $LaMnO_3$, (c) (*1*) $TbMn_2O_5$, and (*2*) $YbMn_2O_5$ clusters filling their intersphere nanocavities.

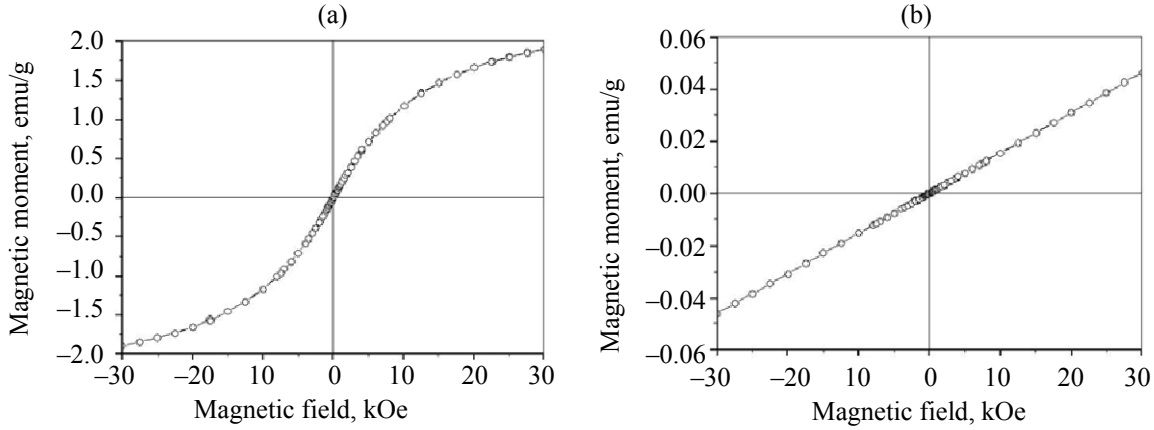

Fig. 15. (a) Hysteresis loop and (b) magnetization curve of the opal matrix with $LiCoPO_4$ clusters filling its intersphere nanocavities.

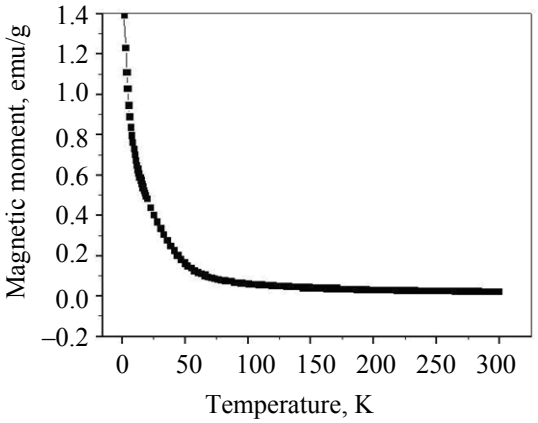

Fig. 16. Temperature dependence of magnetization, measured at 1 kOe, for the opal matrix with $GdMn_2O_5$ clusters filling its intersphere nanocavities.

(10–15 nm). The efficient interaction of microwave fields with metal nanoparticles is of interest for finding conditions of the existence of a negative real magnetic susceptibility, as well as in terms of application in SHF electronic devices.

The *dc* magnetic susceptibilities and the *ac* magnetic susceptibilities measured at 1 kHz completely coincide with each other, implying a lack of contribution into the *ac* magnetic susceptibility of bound changes that might arise due to the magnetoelectric effect.

Magnetization curves and hysteresis loops, as well as temperature dependences of magnetic moment were measured for magnetite- (Figs. 16 and 17) and titanate-filled opal matrices (Fig. 18). Contraction of the central portion of the hysteresis loop was observed (Fig. 18a, T = 2 K). The temperature dependence of magnetic moment, measured at 1 kOe, has a steep- (up to $T \sim 25-40$ K) and a slow-decline portions ($T > 50$ K). The temperature dependence of magnetic susceptibility shows an analogous behavior, specifically, the magnetic moment decreases with temperature; therewith, no signs of phase transitions are observed. The temperature dependences of magnetization, measured in the *ac* field at 1 kHz, reveal the tendencies of both the real and imaginary magnetic moments to decrease with temperature. The curve pattern (but not the ordinate value) for an ordinary dielectric material should be the same as in the case of *dc* measurements, which is explained by the interaction of different fields.

The temperature dependences of phase shift for the real and imaginary magnetizations M' and M'' have a steep-decline portion (up to $T \approx 10$ K). The real and imaginary *ac* magnetic susceptibilities show an analogous temperature dependence. At temperatures higher than 50 K, the imaginary magnetic susceptibility is negligibly low. In the case of the opal matrices filled with $Dy_2Ti_2O_7$, no permeability and eddy currents were observed.

Dielectric Characteristics of Nanocomposites

Real and imaginary dielectric permittivities ε' and ε" were measured for opal matrices with empty nanocavilites and nanocavities filled with 12–28-nm clusters of different substances. Dielectric frequency spectra in a wide frequency range (from 1 MHz to 2 THz) were measured [10]. The components of dielectric permittivity in the high-frequency range (1×10^6–1.8×10^9 Hz) were measured on a dielectric spectrometer with a Novocontrol BDS 2100 sample cell and an Agilent 4291B RF Impedance analyzer.

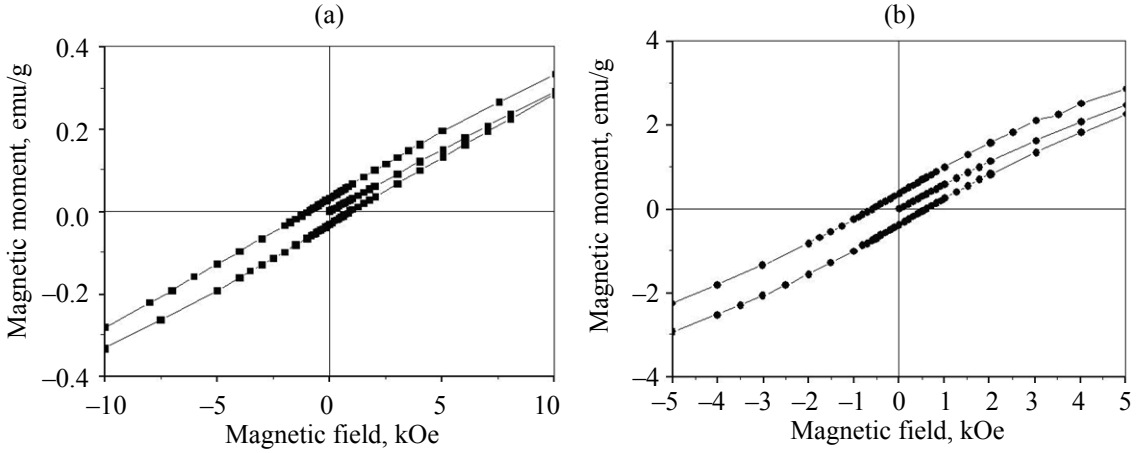

Fig. 17. Fragments of the hysteresis loops for the opal matrices with (a) Bi and Mn compounds (coercive force ~1 kOe) and (b) $TbMn_2O_5$ (coercive force ~600 Oe, T = 2 K) clusters filling their intersphere nanocavities.

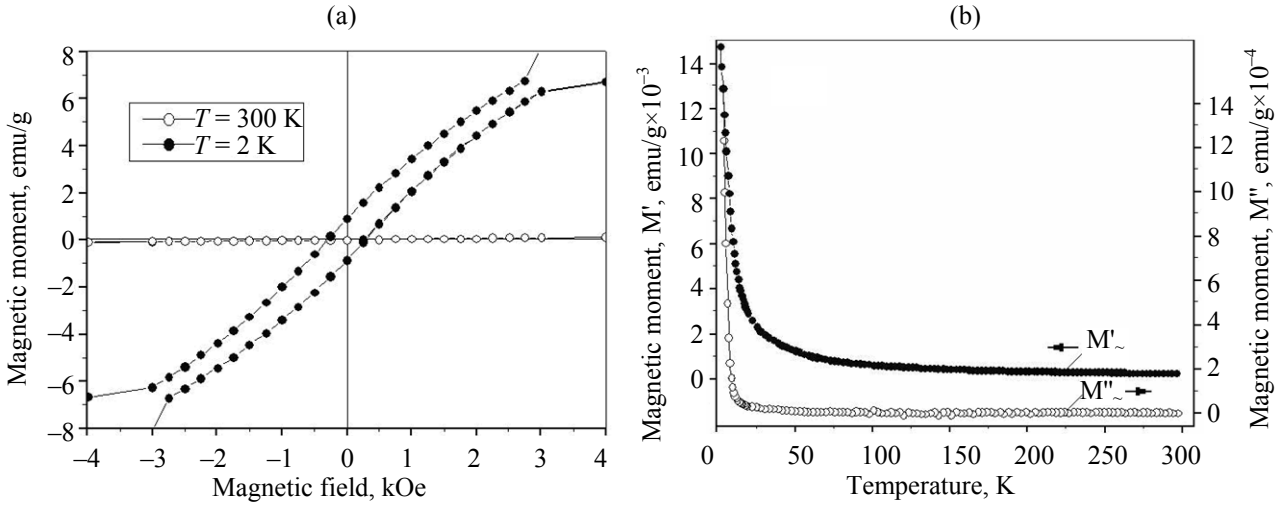

Fig. 18. (a) Hysteresis loops and (b) temperature dependences measured (*ac* measurements at 8 Oe) for the opal matrix with $Dy_2Ti_2O_7$ clusters filling its intersphere nanocavities.

Measurements in the microwave range (2×10^8–2×10^{10} Hz) were performed on an Agilent E8364B network analyzers using an Agilent 85070E open-ended coaxial dielectric probe (Figs. 19–24). Coaxial measurements (1×10^6–1.8×10^9 Hz) were performed on cylinder-shaped samples (diameter 3 mm, height 4–5 mm).

The dielectric losses for the most part of the composites studied are low and almost frequency-independent over the entire frequency range studied. A decline of ε'' toward low frequencies and its rise toward high frequencies was only observed. The dielectric dispersion in the microwave range was only slightly expressed, and all essential changes are likely to occur at lower frequencies. Note that a metamaterial should have not only high ε' values but also low ε'' values (low wave absorption) in a preset frequency range. Consequently, such unusual properties of metamaterials as a negative group velocity of signal propagation (in certain frequency ranges) due to different effects in these materials are especially expressed in the resonance region (unlike what is the case with crystalline materials). Such peculiar features in combination with a low absorption of electromagnetic waves make metamaterials promising candidates for application in SHF electronics and optoelectronics.

The dielectric permittivities ε' of all the opal matrices with the above-mentioned crystal phases embedded in their nanocavities are higher than those of the opal matrix with empty nanocavities. A dielectric dispersion characteristic of composite materials takes place in the entire frequency range, and, therewith, ε' slightly decreases with increasing frequency.

The dielectric losses tend to increase both toward low frequencies (f < 10 MHz) and toward THz frequencies. The slightly enhanced ε' losses are

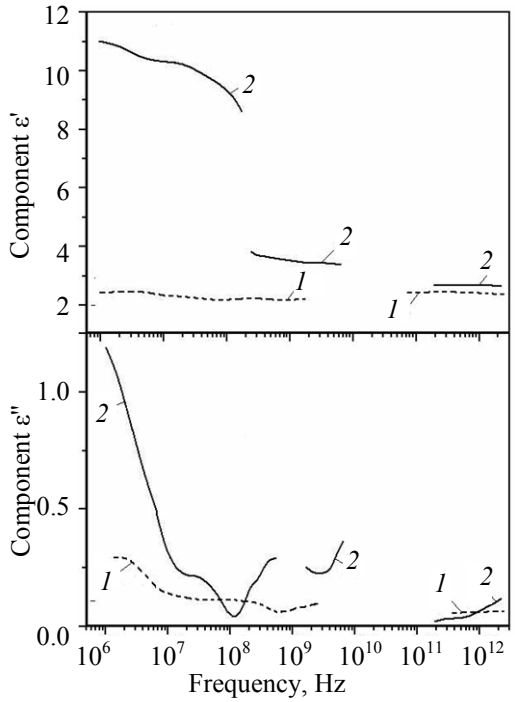

Fig. 19. Frequency dependences of the real (ε') and imaginary (ε'') components of dielectric permittivity in the frequency range 10^6–10^{12} Hz for the (*1*) starting opal matrices and (*2*) opal matrices with $LiCoPO_4$ clusters filling their intersphere nanocavities.

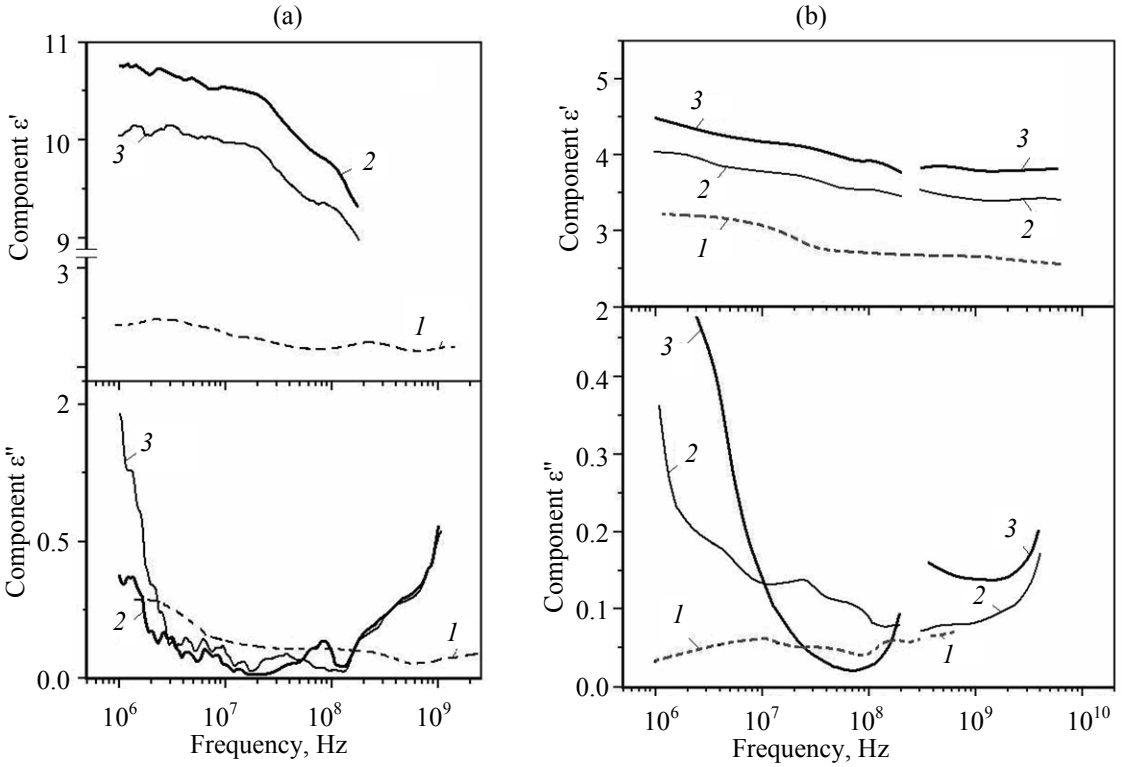

Fig. 20. Frequency dependences of the real (ε') and imaginary (ε'') components of dielectric permittivity in the frequency range 10^6–10^{12} Hz for the (*1*) starting opal matrices and opal matrices with their intersphere nanocavities partially filled with (a, *2*) $GdMn_2O_5$, (a, *3*) $Bi_2Mn_4O_{10}$, (b, *2*) $YMnO_3$, and (b, *3*) $NdMn_2O_5$ clusters.

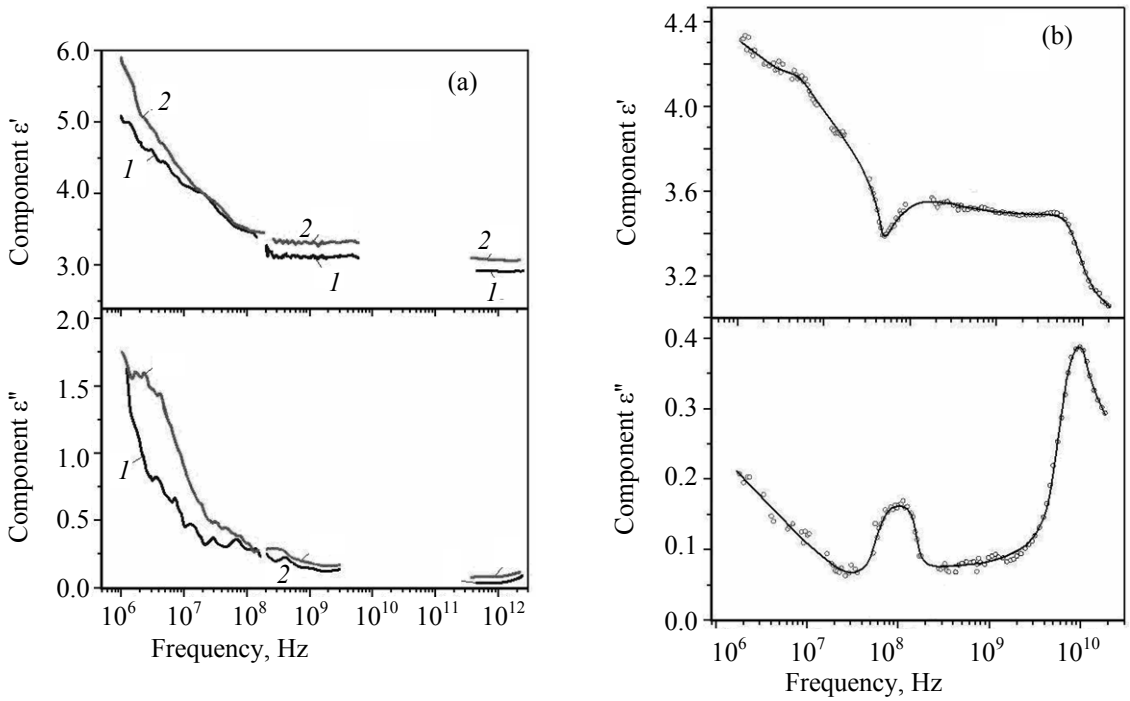

Fig. 21. Frequency dependences of the real (ε') and imaginary (ε'') components of dielectric permittivity in the frequency range 1 MHz–5 THz and in the THz range for the opal matrices with (a) (*1*) $YbMn_2O_5$, (*2*) $ErMn_2O_5$, and (b) $LaMn_2O_5$ clusters filling their intersphere nanocavities.

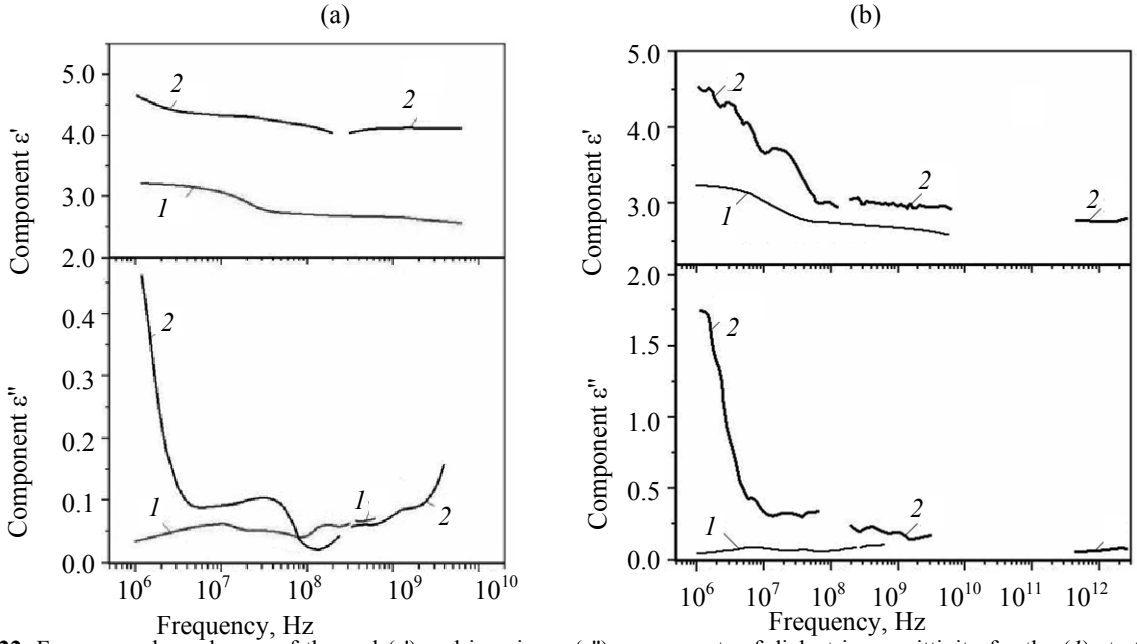

Fig. 22. Frequency dependences of the real (ε') and imaginary (ε") components of dielectric permittivity for the (*1*) starting opal matrices and opal matrices with (a, *2*) Er_2TiO_5 and (b, *2*) $Yb_2Ti_2O_7$ clusters filling their intersphere nanocavities.

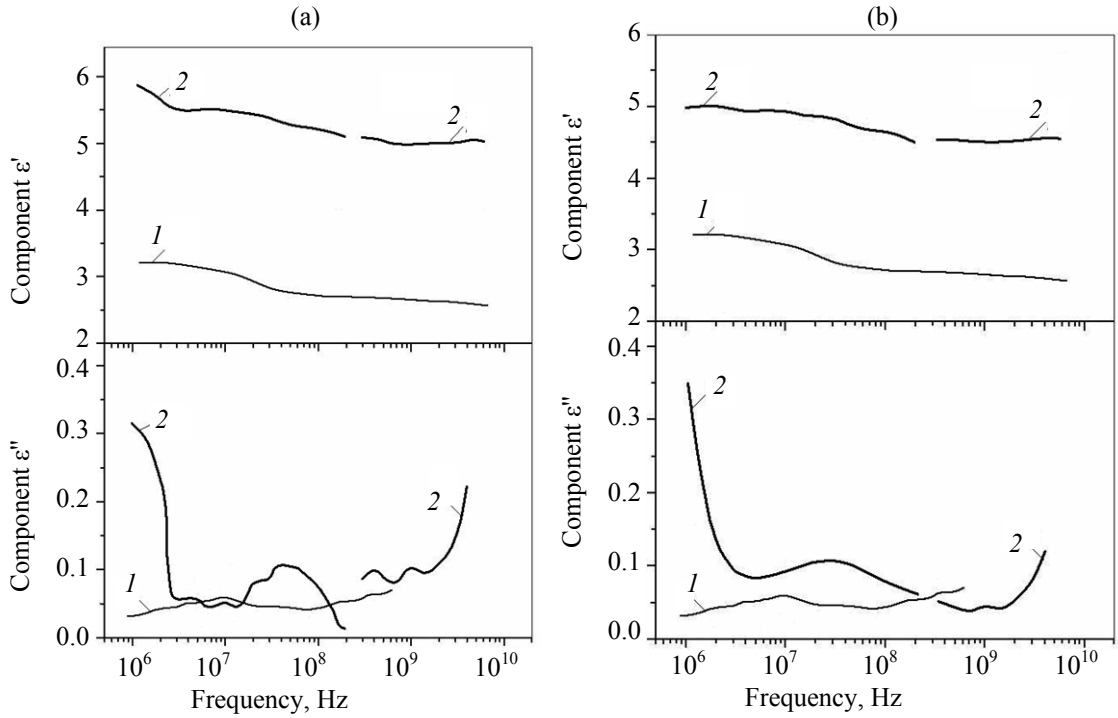

Fig. 23. Frequency dependences of the real (ε') and imaginary (ε") components of dielectric permittivity for the (*1*) starting opal matrices and opal matrices with (a, *2*) $PbTiO_3$ and (b, *2*) $PbTi_3O_7$ clusters filling their intersphere nanocavities.

associated with a contribution of *dc* permittivity, and the increase at high frequencies corresponds to ε' dispersion. The nonmonotonic nature of some frequency dependences can be explained in part by experimental inaccuracies (uncontrolled surface roughness or sample shape and thickness, lack of electrodes, etc.) and by a possible magnetic effect of the materials.

Embedded ZnO, $BaTiO_3$, $PbTiO_3$, and $PbTi_3O_7$ clusters increase the ε' values of opal matrices by 40–

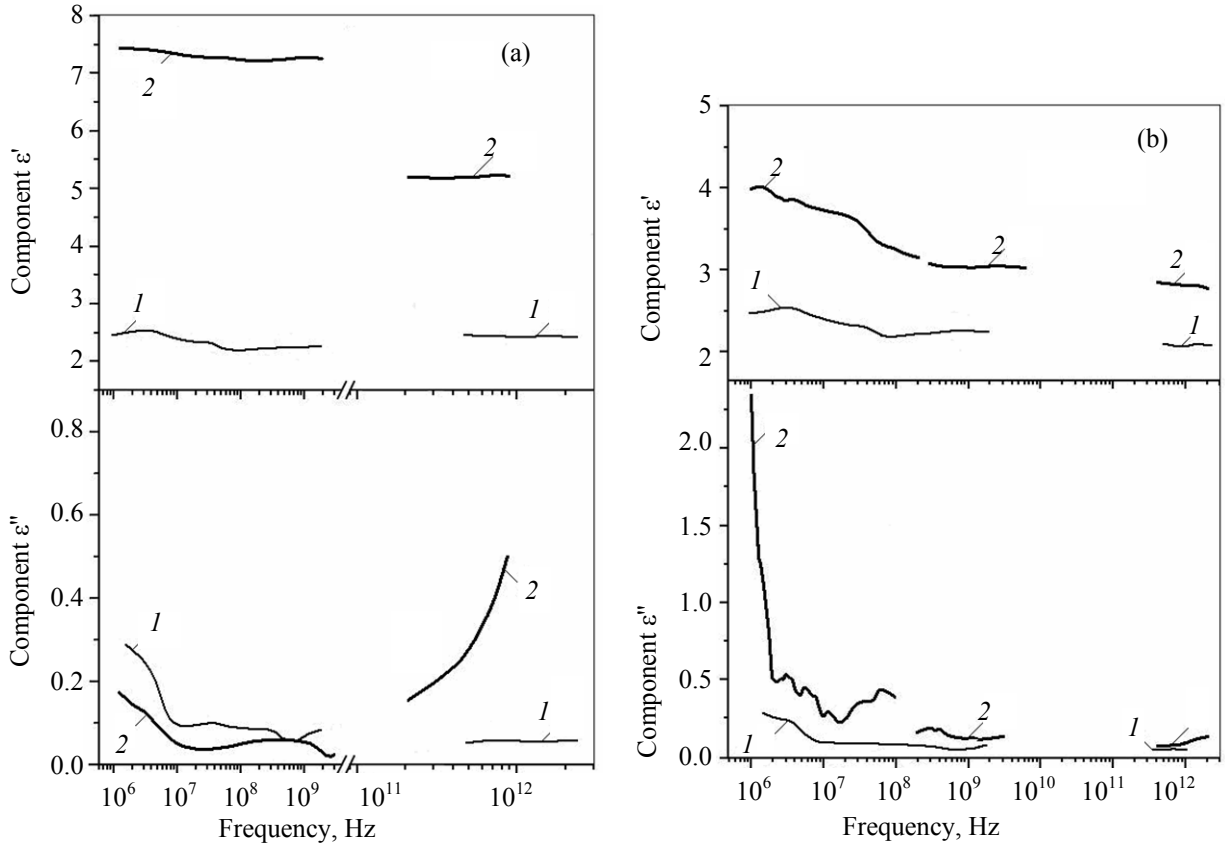

Fig. 24. Frequency dependences of the real (ε') and imaginary (ε'') components of dielectric permittivity for the (*1*) starting opal matrices and opal matrices with (a, *2*) $BaTiO_3$ and (b, *2*) ZnO clusters filling their intersphere nanocavities.

200% (1–5 units) but have no effect on the dielectric losses which still remain low (ε'' < 0.1) over an almost entire frequency range studied. Notable only are increased dielectric losses at low (10^6 Hz) and high frequencies (10^{10}–10^{12} Hz). In the first case this can be explained by the presence of some water in matrix nanocavities, while the increased dielectric losses in the THz range is of a more basic nature and associated with the low-frequency wing of the phonon spectrum of the embedded compounds. The most evident increase of dielectric losses with increasing frequency in the THz range takes place in the case of $BaTiO_3$- and $PbTiO_3$-filled matrices, on account of the fact that the phonon spectra of the crystal phases of these compounds contain a low-frequency (~3 THz) segnetoelectric phonon mode [7].

In the microwave range (10^6–10^{10} Hz), no significant ε' dispersion is observed, which correlates with low microwave losses, whereas the minor differences in the ε' values measured in the MHz and THz ranges for the nanocomposites containing $BaTiO_3$ clusters are likely to be explained by a concentration gradient of the $BaTiO_3$ clusters in the opal matrix (from the subsurface regions to center) and by a lack of a constant crystallographic orientation of crystallites of the embedded substance with respect to the electric field gradient in the megahertz and terahertz experiments.

The fact that opal matrices filled with ZnO, $BaTiO_3$, $PbTiO_3$, and $PbTi_3O_7$ clusters acquire increased dielectric permittivity but preserve low dielectric losses in the microwave range explain the enhanced interest in research on such nanocomposites as a stage of the search for and subsequent creation of novel metamaterials.

CONCLUSIONS

Nanocomposites on the basis of opal matrices with titanate $R_2Ti_2O_7$ or R_2TiO_5 nanoparticles (R = Yb, Tb, Er, La, Dy, Pr, Gd, or Nd) embedded in their intersphere nanocavities are promising candidates for application in magnetically controlled devices. The study of the structure, composition, and dielectric properties of the developed metamaterials on the basis

of opal matrices filled with electrically active substances (ZnO, $BaTiO_3$, and $PbTiO_3$ piezo- and segnetoelectrics) provided necessary data for the development of physicochemical foundations for the production and application of noncrystalline spatially inhomogeneous materials with nanometer range–modulated electric and dielectric parameters.

The proposed R@D approach to such metamaterials will be the most efficient in the development of solid-state SHF devices (filters, delay lines, phase inverters, and other portable and power-efficient control units), as well as devices for controlling the group velocity of signal propagation, which make use of different effects in chiral metamaterials (optical delay lines, multichannel multiplexers/demultiplexers, etc.).

ACKNOWLEDGMENTS

The work was financially supported in part by the Russian Foundation for Basic Research (project ofi-m-2011 no. 11-02-12095) and the Presidium of the Russian Academy of Sciences, as well as the Czech Science Foundation (project no. P204/12/0232). The authors are grateful to A.V. Korolev for magnetic measurements of nanocomposites at the Center for Collective Use, Institute of Metal Physics, Ural Branch, Russian Academy of Sciences.

REFERENCES

1. Sarychev, A.K. and Shalaev, V.M., *Electrodynamics of Metamaterials,* Singapore: World Scientific and Imperial College Press, 2007.
2. Kong, J.A., *PIER*, 2002, vol. 35, pp. 1–52.
3. *Nanomaterialy. III. Fotonnye kristally i nanokompozity na osnove opal matrits* (Nanomaterials. III. Photonic Crystals and Nanocomposites on the Basis of Opal Matrices), Samoilovich, M.I., Ed., Moscow: Tekhnomash, 2007.
4. Samoilovich, M.I., Belyanin, A.F., Kleshcheva, S.M., and Tsvetkov, M.Yu., *Nauka Teknol. Prom-sti*, 2010, no. 4, pp. 73–84.
5. Samoilovich, M.I., Bovtun, V., Rinkevich, A.B., Belyanin, A.F., Kleshcheva, S.M., Kempa, M., and Nuzhnyy, D., *Inzh. Fiz*., 2010, no. 6, pp. 29–38.
6. Samoilovich, M.I., Bovtun, V., Belyanin, A.F., Tsvetkov, M.Yu., Kleshcheva, S.M., Kempa, M., and Nuzhnyy, D., *Nanoinzheneriya*, 2011, no. 2, pp. 32–38.
7. Samoilovich, M.I., Rinkevich, A.B., Bovtun, V., Belyanin, A.F., Nuzhnyy, D., Kempa, M., Kleshcheva, S.M., *Nanoinzheneriya*, 2012, no. 3(9), pp. 22–30.
8. Samoilovich, M.I. and Talis, A.L., *Nano-Mikrosistem. Tekh*., 2012, no. 1, pp. 31–36.
9. Ustinov, V.V., Rinkevich, A.B., Perov, D.V., Samoilovich, M.I., and Kleshcheva, S.M., *J. Magnetism Magnet. Mater.*, 2012, vol. 324, pp. 78–82.
10. Nuzhnyy, D., Vanek, P., Petzelt, J., Bovtun, V., Kempa, M., Gregora, I., Savinov, M., Krupkova, R., Studnicka, V., Bursik, J., Samoylovich, M.I., and Schranz, W., *Proc. Appl. Ceram*., 2010, vol. 4, pp. 215–223.